Nano Energy (2015) 16, 399–407

Available online at www.sciencedirect.com

ScienceDirect

journal homepage: www.elsevier.com/locate/nanoenergy

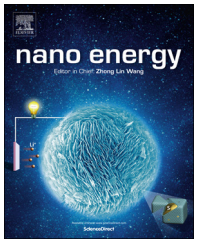

SnO_2 coated carbon cloth with surface modification as Na-ion battery anode

Yihang Liu[a,1], Xin Fang[b,1], Mingyuan Ge[b], Jiepeng Rong[b], Chenfei Shen[b], Anyi Zhang[b], Hani A. Enaya[c,d], Chongwu Zhou[a,*]

[a]*Department of Electrical Engineering, University of Southern California, Los Angeles, CA 90089, United States*
[b]*Department of Chemical Engineering and Material Science, University of Southern California, Los Angeles, CA 90089, United States*
[c]*Department of Electrical Engineering, University of California at Los Angeles, Los Angeles, CA 90095, United States*
[d]*King Abdulaziz City for Science and Technology, Riyadh, Saudi Arabia*

Received 19 March 2015; received in revised form 6 July 2015; accepted 9 July 2015
Available online 26 July 2015

KEYWORDS
Sodium-ion batteries;
Carbon cloth;
Surface coating;
Atomic layer deposition;
Carbon coating;
Tin dioxide

Abstract
Sodium (Na)-ion batteries offer an attractive option for low cost large scale energy storage due to the earth abundance of Na. SnO_2 is considered as a high capacity anode for Na-ion batteries with a theoretical capacity of 1378 mA h/g. However, several limitations, such as large volume expansion with cycling, slow kinetics and low electrical conductance, have severely limited its performance. In this article, we demonstrate an anode consisting of a SnO_2 nanocrystal layer grown on hierarchical microfibers of carbon cloth (CC) with extra surface coating to addresses the above challenges associated with SnO_2 anodes. The soft nature of CC and the nanocrystal structure of SnO_2 layers can effectively accommodate the volume change associated with the sodiation process. In addition, the effect from an extra coating layer of carbon ($C/SnO_2/CC$) and Al_2O_3 ($Al_2O_3/SnO_2/CC$) have been explored and the results showed that the extra coating layer can further enhance the performance of SnO_2 anode. The $C/SnO_2/CC$ core-shell structure anode achieved a 501 mA h/g and a 144 mA h/g capacity at 0.1 C and 30 C charge/discharge rate, respectively. Meanwhile, a 375 mA h/g specific capacity after 100 deep cycles with an 80% retention is achieved by $Al_2O_3/SnO_2/CC$ anode. The designed surface-coating/nanocrystal-active-material-layer/conductive-soft-platform core-shell system paves the way to high performance Na-ion batteries.

*Corresponding author.
E-mail address: chongwuz@usc.edu (C. Zhou).
[1]These authors contributed equally.

http://dx.doi.org/10.1016/j.nanoen.2015.07.010
2211-2855/

Introduction

Li-ion batteries have been considered as one of the most promising candidates for energy storage due to their high energy density and cycle stability [1,2]. As an alternative technology, Na-ion batteries potentially offer a lower cost, safer and more environmental friendly battery system in comparison with Li-ion system. Several promising cathode material with high energy density and cycling stablility have been well developed, such as layered sodium transition-metal oxides[3,4], phosphates/fluorophosphates[5,6] and Prussian blue type materials[7,8]. On the other hand, anode part becomes the main drawback of the commercialization of the Na-ion batteries because typical graphite employed in Li-ion batteries do not intercalate Na^+ ions, which is related to the large size of the Na-ion, which is 372% that of a Li-ion , and thus makes it impossible to simply adopt the recent knowledge and strategies developed for high performance Li-ion batteries directly onto Na-ion batteries.[9] Anode materials that have been investigated include metal oxides[10], alloys[11] and carbonaceous materials[12]. Sn is a promising anode material because it alloys with Na at a high specific capacity of 847 mA h/g when $Na_{15}Sn_4$ is formed [13]. Several studies of Sn film and nanostructured anodes were reported with capacities up to 405 mA h/g after 150 cycles [14,15]. On the other hand, SnO_2 can deliver a high theoretical sodium storage capacity of 1378 mA h/g, but with the same volume variation problem as Sn metal, and hence further surface treatment or matrix scaffold is needed to stabilize SnO_2 anode and improve the electronic conductivity [16,17]. Recently developed SnO_2@graphene nanocomposites have improved cycling performance, but this method lacks the processability and rate capability because of the high cost of graphene [18].

In this study, we demonstrate a surface-coating/nanocrystal-active-material-layer/conductive-soft-platform multilayer nanocomposite microfiber electrode by using atomic layer deposition (ALD), hydrothermal synthesis method and carbon cloth (CC) as a soft platform to solve the problems mentioned above, as demonstrated in Figure 1. More specifically, we have developed a binder-free multilayer nanocomposite core-shell microfiber electrode consisting of a hydrothermal synthesized SnO_2 nanocrystal layer on conductive carbon cloth (SnO_2/CC) with surface coatings. The carbon fibers in carbon cloth are intrinsically soft and porous based on the layered structure with strong interlayer interactions and weak van der Waals interplanar interactions between adjacent graphene sheets [19]. As the core of the core-shell structure, during the sodiation and de-sodiation process, the soft carbon fibers can change in shape to prevent the pulverization of the active material, and the pores in the fiber together with the aligned core–shell array structure can also provide extra space to accommodate the volume change to avoid the detachment of the active material layer. An ALD Al_2O_3 coating and a hydrothermal carbon coating are further applied on SnO_2/CC electrodes to enhance the cycle life and rate capability. The comparison of impedance and morphology between fresh and cycled electrodes revealed the mechanism of capacity decay and how Al_2O_3 surface coating can protect the active material layer. The hierarchical core-shell SnO_2 anode with designed surface-coating/nanocrystal-active-material-layer/conductive-soft-platform structure described is ideal for high power and large scale sodium ion storage. The hydrothermal synthesis, ALD technology and conductive fiber substrates are scalable for large throughput manufacturing.

Experimental

Materials preparation

SnO_2 coating was synthesized through hydrothermal reaction. 0.1 mol/L $SnCl_2$ was dissolved into 5 ml ethanol and 15 ml DI water, then 1ml HCl acid was added. Oxidized carbon cloth was immersed into the SnO_2 precursor solution overnight in Teflon autoclave and followed by heat treatment at 110 °C for 6 h. Obtained SnO_2/CC was washed in DI water and ethanol carefully then dried overnight. The weight of SnO_2 was measured by checking the weight of carbon cloth (CC) before and after SnO_2 hydrothermal deposition. The loading mass density of the SnO_2 is $\sim$ 0.9 mg/cm^2 which is calculated by using the weight of SnO_2 divided by the area of the carbon cloth.

Carbon coating process was completed using a hydrothermal method, SnO_2 coated carbon cloth was immersed into 0.1 mol/L sucrose solutions, and then transferred into a Teflon autoclave and heated up to 250 °C for 3 h. Obtained C/SnO_2/CC was washed in DI water and then annealed at 500 °C for half an hours. The Obtained C/SnO_2/CC was washed in DI water and dried in air, then annealed at 500 °C for half an hour in argon gas.

The ALD Al_2O_3 coating was performed on the fabricated SnO_2/CC electrode with a homemade ALD system at the temperature of 90 °C and pressure of 6×10^{-1} torr in a vacuum chamber.

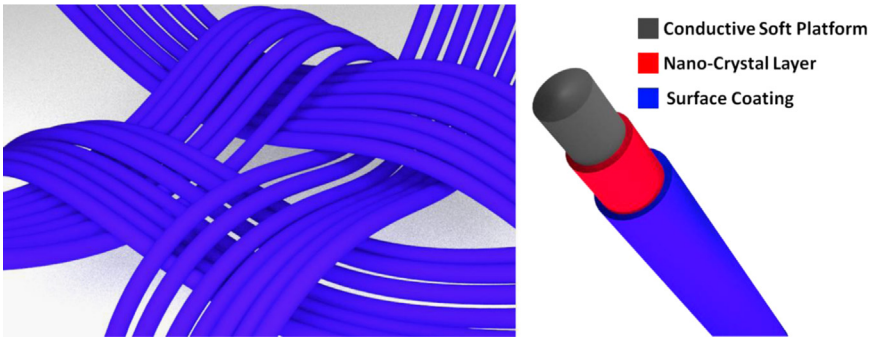

Figure 1 Schematic figure of surface-coating/nanocrystal-active-material-layer/conductive-soft-platform structure.

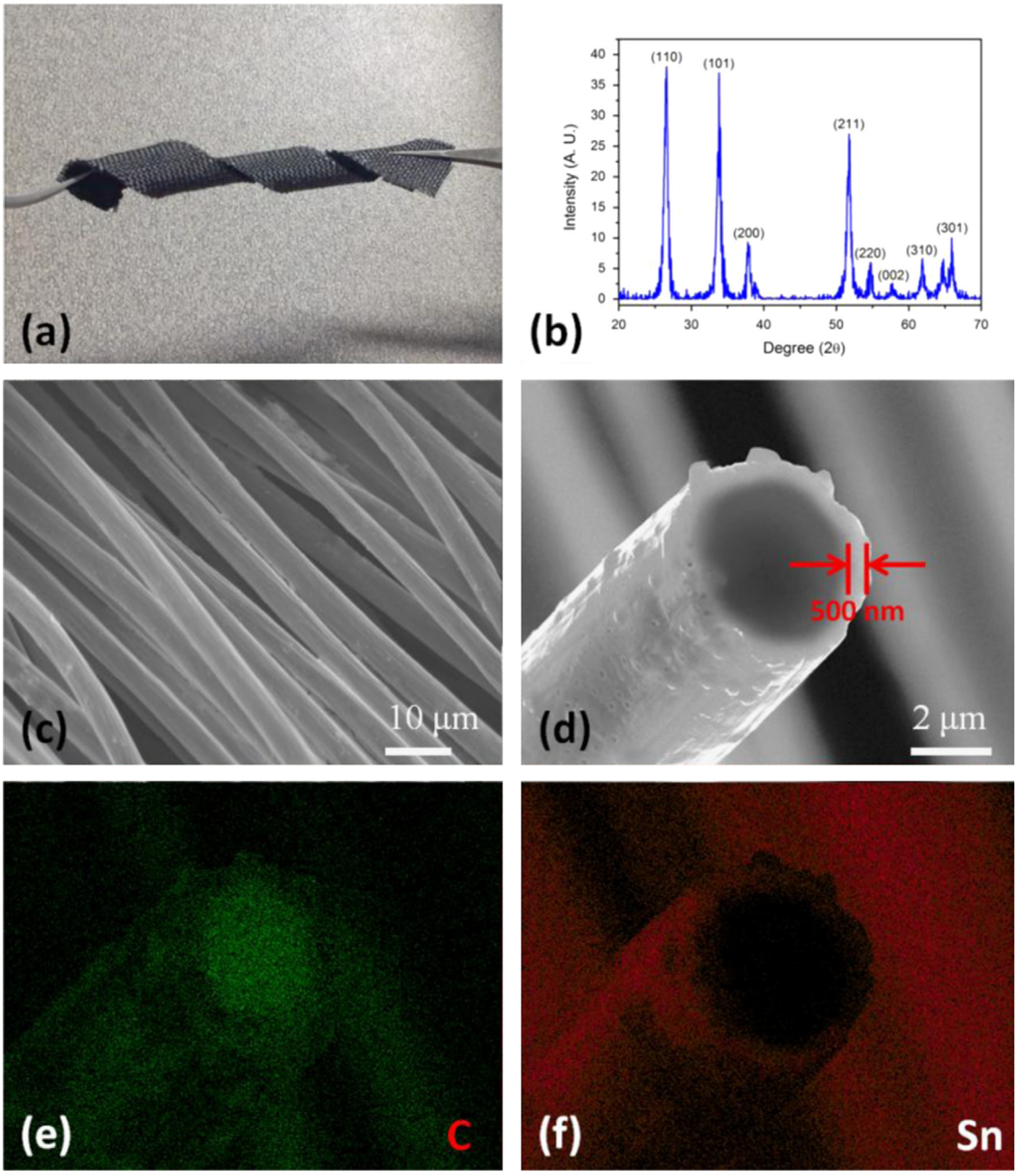

Figure 2 (a) Optical image of flexible SnO_2/CC binder free electrode, (b) XRD profile of hydrothermal synthesized SnO_2, (c) SEM image of SnO_2/CC and (d) cross section SEM image of a single SnO_2/CC fiber and its EDX element mapping profile of carbon (e) and tin (f).

Electrochemical measurements

The SnO_2 electrodes were cut into 1×1 cm^2 pieces and tested in half cells configuration with Na metal as counter electrodes and 1 M $NaPF_6$ in polycarbonate (PC) electrolyte with 5% FEC by vol. as additive. The batteries were cycled in the voltage range of 0.1–2.5 V at room temperature. Electrochemical impedance spectra (EIS) were collected with AC voltage at 5 mV amplitude and frequency range of 100 kHz–10 mHz. The batteries were fully charged and then rested to reach equilibrium before the impedance test. All electrochemical experiments were conducted at room temperature, and all capacities were calculated based on the weight of SnO_2.

Results and discussion

The carbon fibers are initially treated with nitric acid to enrich the hydroxyl (–OH) groups on its surface, which can provide strong hydrogen bonding between the fiber and active material. A thin layer of SnO_2 was then synthesized onto carbon cloth using the hydrothermal method, the resulted flexible and binder free electrode is shown in Figure 2a and is denoted as SnO_2/CC. In Figure 2b, the crystal structure of hydrothermal synthesized SnO_2 is confirmed by X-ray diffraction (XRD), and no impurity is detected from the XRD pattern.

The hierarchical structure of SnO_2/CC is illustrated in the SEM image (Figure 2c). All of the SnO_2/CC fibers have a

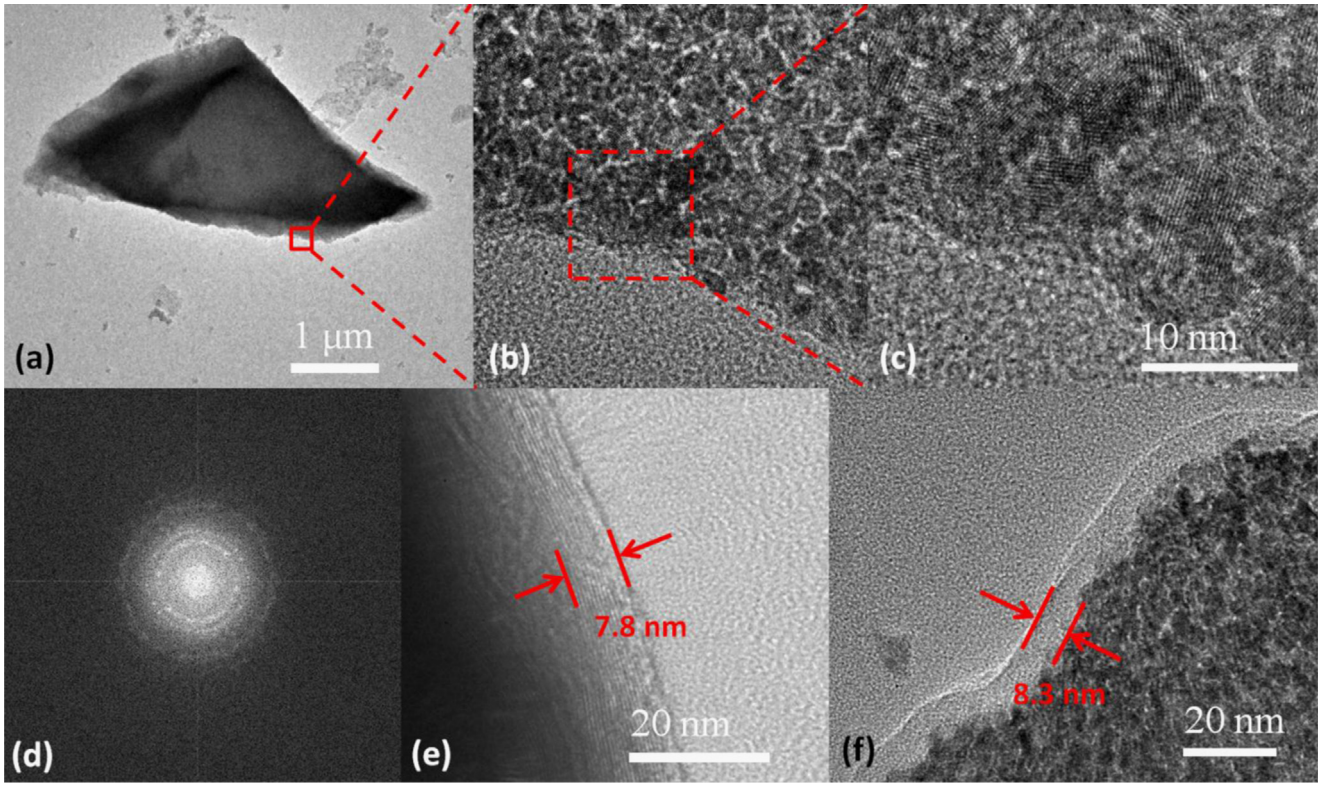

Figure 3 (a) TEM image of a large bulk piece of SnO_2 layer coated on CC, (b, c) High resolution TEM image of SnO_2 nanocrystal at different magnification, (d) FFT image of the area marked in (b). TEM images of the carbon layer (e) and Al_2O_3 layer (f) coated on CC.

diameter on the order of 5 μm uniformly. In order to confirm the hierarchical core-shell structure of the nanocomposite microfiber, the freshly cut SnO_2/CC sample was further characterized in detail. In Figure 2d, a SnO_2 shell layer with a thickness of ~500 nm is marked on the cross-section SEM image. Figure 2e and f shows the EDX mapping profiles of the carbon and tin elements in Figure 2d, both of which show a good agreement with the contrast profile of Figure 2d. Both SEM images and EDX mapping cooperatively reveal that all carbon fibers are coated with a SnO_2 layer uniformly to form SnO_2/CC hierarchical core-shell nanocomposite microfibers. Similar core-shell structure with conductive core has been proven effective in resolving issues associated with electron-transfer kinetics along the high aspect-ratio rod- or wire-like materials [20,21]. Compared to conventional rigid metallic substrates, the carbon cloth is extremely soft and porous with a high capacity for electrolyte absorption which can provide a dual diffusion channel for Na-ions. In order to study the effect of substrate and surface coating on electrochemical performance, additional sucrose hydrothermal carbon coating and ALD Al_2O_3 coating are also applied on the SnO_2/CC samples and are denoted as C/SnO_2/CC and Al_2O_3/SnO_2/CC, respectively.

The hierarchy, crystalline and configuration of SnO_2/CC nanocomposite with different surface coatings were further confirmed by transmission electron microscopy (TEM). In Figure 3a, the TEM image shows a large bulk piece from the SnO_2 cylindrical active material shell layer coated on a single carbon fiber. According to the high resolution TEM image shown in Figure 3b and the FFT image (Figure 3d) of the area marked in Figure 3b, the SnO_2 layer is polycrystalline with uniform grain size at ~5 nm. The high-resolution TEM images of carbon and Al_2O_3 surface coatings are shown in Figure 3e and f. Several carbon layers are observed in Figure 3e, the thickness of the carbon coating is 7.8 nm, which is partially graphitized after the annealing. In Figure 3f, the thickness of the uniform ALD Al_2O_3 coating is ~8.3 nm and in an amorphous nature. In order to study the degree of graphitization of the carbon coating, we designed the following control experiment and characterized the annealed sample with Raman spectrum equipped with a 532 nm laser source. Sucrose solution with 0.1 mol/L concentration was dropped onto a quartz substrate and dried in air, and then the substrate was annealed at 500 °C for half an hour in argon gas. The Raman spectrum is presented in Figure S1 (Supporting Information). The peaks of D and G bands were centered at 1359 cm^{-1} and 1595 cm^{-1}. The D band is correlated with structural defects and disorder-induced features in the graphene layers of carbon materials, while the G band is indicative of the high frequency E_2g first-order graphitic crystallites of carbon. The ratio between the intensity of the G and D bands is 1.51.

The cycling performance of SnO_2/CC, C/SnO_2/CC and Al_2O_3/SnO_2/CC electrodes was investigated by galvanostatic charge and discharge of the electrodes between 0.05 and 2.5 V at the current density of 0.1 C (134 mA/g), and the results are shown in Figure 4a. Electrodes assembled in a traditional way by mixing carbon black, PVDF binder and commercial SnO_2 powder were also tested for comparison. The commercial SnO_2 powder suffered from rapid capacity decay, retaining only 6% of the initial capacity after 10 cycles (Figure S2,

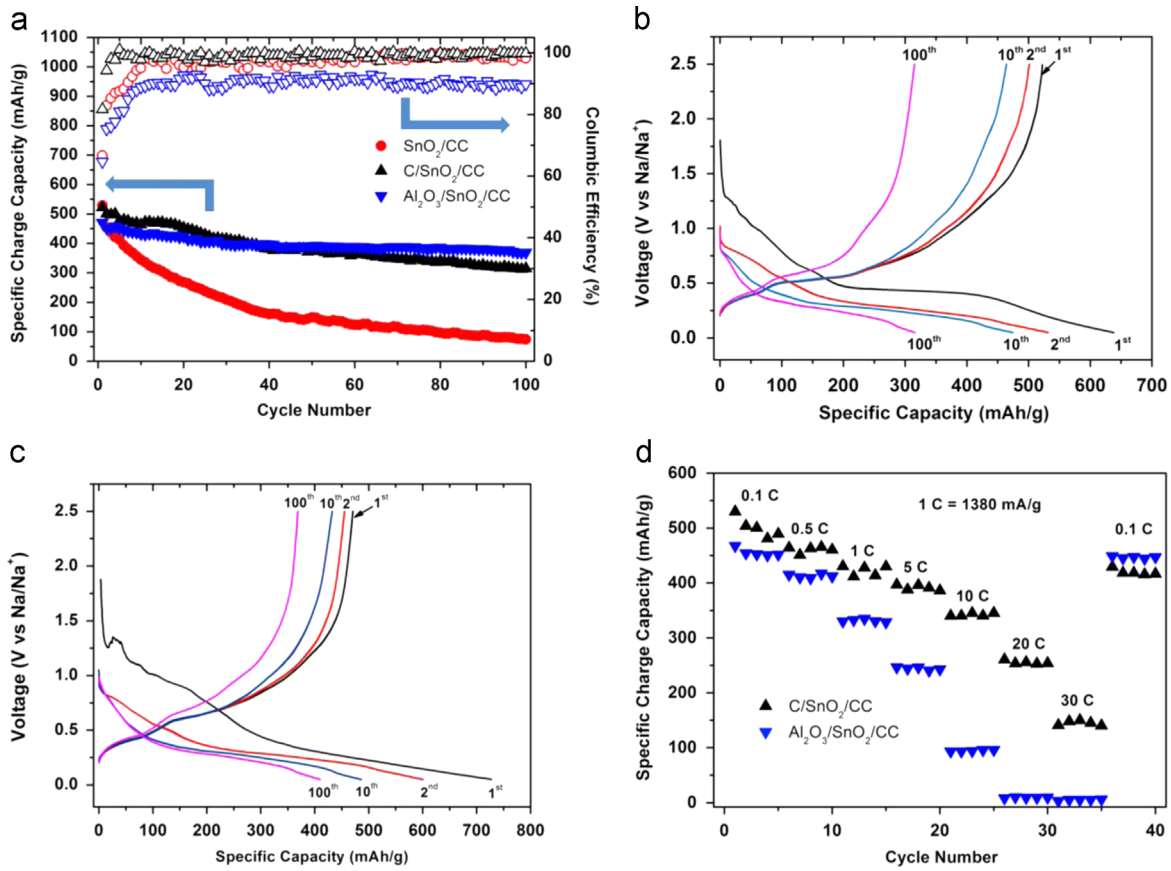

Figure 4 (a) Cycling stability and Coulombic efficiency of SnO_2/CC, C/SnO_2/CC and Al_2O_3/SnO_2/CC. Potential profiles of (b) C/SnO_2/CC and (c) Al_2O_3/SnO_2/CC in cycling test. (d) Rate performance of C/SnO_2/CC and Al_2O_3/SnO_2/CC.

Supporting information), which is mainly because of the large volume change of SnO_2 during sodiation process and resulted in the detachment of the active material [22]. In contrast, for the SnO_2/CC sample without any surface coating, its initial specific charge capacity is 529 mA h/g and it maintains 30% of initial capacity after 40 cycles, which is an obvious improvement over the conventional electrodes made of commercial SnO_2 powder. The degradation was suppressed because the high surface area, porous structure and the intrinsic soft characteristics of carbon cloth can effectively accommodate the volume charge during sodiation and de-sodiation process [23,24]. After 40 cycles, the capacity decay becomes slower and finally the capacity reaches 74 mA h/g at the 100th cycle. The cycling stability is further enhanced by a thin layer of carbon and Al_2O_3 coating. The C/SnO_2/CC sample reaches a 522 mA h/g initial charge capacity which is similar to the SnO_2/CC sample without any surface coating, but it shows a 60% retention which is much higher than the SnO_2/CC sample. This demonstrates that the designed surface-coating/nanocrystal-active-material-layer/conductive-soft-platform structure can greatly suppress the volume change and the pulverization of SnO_2 crystal to improve the cycling stability. Meanwhile, although the Al_2O_3/SnO_2/CC anode has a 470 mA h/g initial capacity which is slightly lower than C/SnO_2/CC, it shows the best retention of 80% and delivers a 377 mA h/g capacity which is even 63 mA h/g higher than C/SnO_2/CC after 100 cycles. This is a reasonable result since the Al_2O_3 layer is much denser than carbon layer and can provide the best mechanical support to the SnO_2/CC core shell electrode [25,26]. The capacity comes from the carbon cloth is proved negligible (Figure S3, Supporting information). For the SnO_2/CC anode, the efficiency reaches around 98% in 11 cycles, however, the efficiency of the C/SnO_2/CC anode quickly increased to above 99% in the first 3 cycles benefiting from the excellent electronic conductivity from the carbon coating. The Al_2O_3/SnO_2/CC anode shows a lower Columbic efficiency than the other two samples, which may be due to the dense and insulate nature of the Al_2O_3 layer.

Aside from capacity, cycling potential profiles of C/SnO_2/CC and Al_2O_3/SnO_2/CC anodes for Na-ion batteries at 1, 2, 5, 10, 50 and 100th cycle are depicted in Figure 4b and c. All curves shown in the two figures represent the typical reaction between SnO_2 and Na, and they also reveal that the additional surface coating processes did not reduce SnO_2 to SnO or Sn metal. For the C/SnO_2/CC anode, potential plateaus in discharge and charge curves gradually disappeared, suggesting that part of the SnO_2 layer disintegrated and detached electronically from the carbon cloth. Comparing to the C/SnO_2/CC anode, the Al_2O_3/SnO_2/CC anode suffers a larger hysteresis between charge and discharge curves due to the insulating Al_2O_3 coating. However it maintained these distinct step plateaus even after 100 deep cycles, which is a much pronounced difference comparing with the carbon coated samples. For the Al_2O_3/SnO_2/CC anode, a bump located around 1.3 V is observed on the first

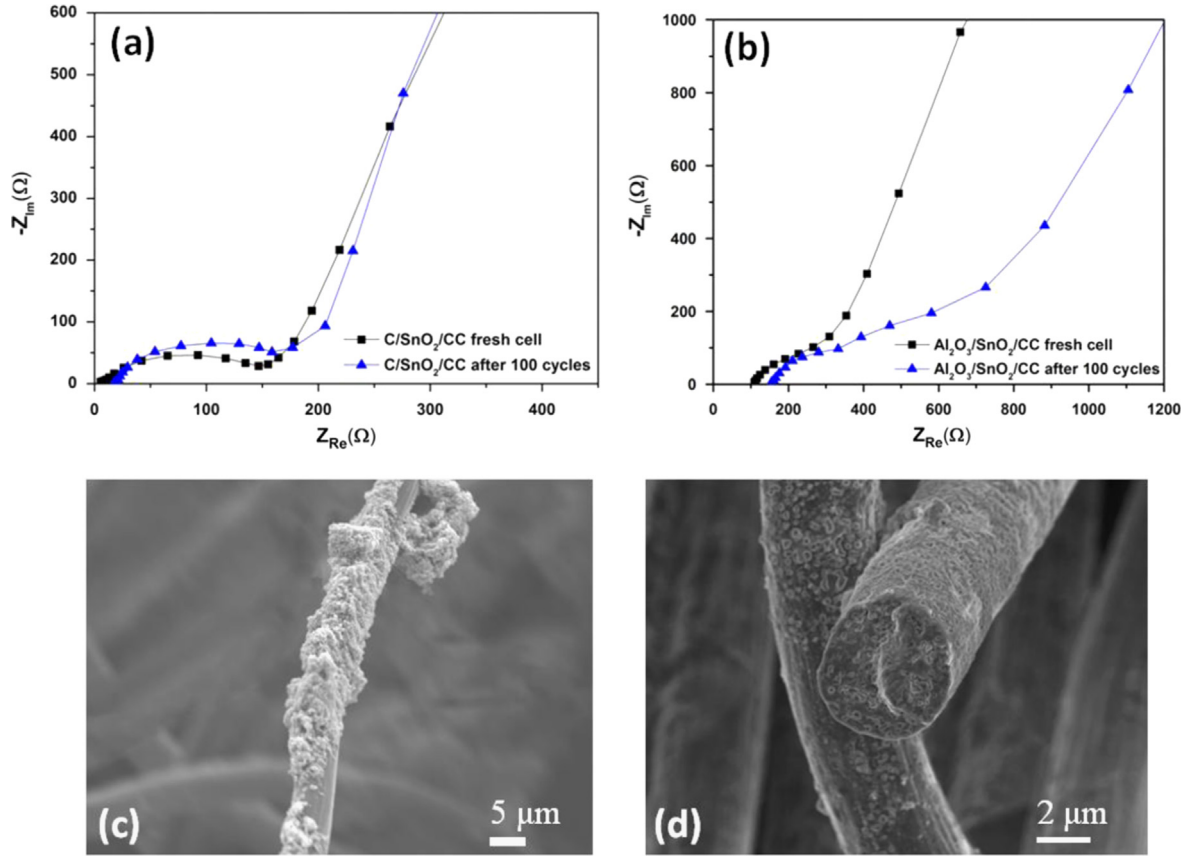

Figure 5 The electrochemical impedance spectrum (EIS) profiles of (a) $C/SnO_2/CC$ and (b) $Al_2O_3/SnO_2/CC$ fresh cell and cell after 100 cycles. The SEM images of (c) $C/SnO_2/CC$ and (d) $Al_2O_3/SnO_2/CC$ after 100 cycles.

discharge curve, which can be considered as the stress release happened between the Al_2O_3 surface coating layer and the SnO_2 nanocrystal layer during the sodiation process, since no similar peak is observed from the $C/SnO_2/CC$ sample. It is clear that graphite carbon layer and dense Al_2O_3 layer are not as soft as the carbon cloth fibers, the stress introduced by the first sodiation process may lead to the activation of the carbon fibers, reconstruction of the active material layer and creating more contact between the active material and electrolyte [27]. The Al_2O_3 coating has been shown as an excellent coverage and conformal deposition on different materials even on Si, [28,29] which has significant volume expansion and contraction during the ion insertion and extraction. The TEM image clearly showed the conformal coating of Al_2O_3 and the electrochemical performance before and after Al_2O_3 coating, which revealed that the Al_2O_3 coating prevents the mechanical degradation of SnO_2 and also explains the cycling stability improvement of the $Al_2O_3/SnO_2/CC$ sample.

In Figure 4d, the rate capability test results show that the $C/SnO_2/CC$ anode can deliver average capacities of 501, 460, 422, 391 and 342 mA h/g at 0.1, 0.5, 1, 5 and 10 C charge/discharge rate. Even at a 20 C and 30 C charge/discharge rate, a 255 mA h/g and a 144 mA h/g specific charge capacities are obtained. For the $Al_2O_3/SnO_2/CC$ sample, slightly lower capacities are observed at different current rates compared to the $C/SnO_2/CC$ sample: a 455 mA h/g average capacity at 0.1 C rate, followed by 413, 331, 245 and 95 mA h/g at 0.5, 1, 5 and 10 C charge/discharge rates. At 20 C and 30 C, the $Al_2O_3/SnO_2/CC$ anode gives very low capacities (<10 mA h/g) and there is no typical potential plateau of SnO_2 on the charge/discharge curves. When the rate was restored to 0.1 C, the $Al_2O_3/SnO_2/CC$ anode showed excellent stability with a 447 mA h/g average capacity which is 27 mA h/g higher than that of the $C/SnO_2/CC$ anode. Obviously, due to the high electrical conductivity of the carbon cloth platform, both carbon and Al_2O_3 coated samples gain fast charge/discharge capability. Especially for the $C/SnO_2/CC$ sample, the conductive carbon fiber core and carbon coating shell provide dual channels for electron transfer and acquire supreme fast charge–discharge capability. The good rate capability can also be partially ascribed to the nano-polycrystalline nature of the SnO_2 active material layer, since the boundaries between crystal grains can provide faster diffusion channels for ions [30,31].

The electrochemical impedance spectrum (EIS) of $C/SnO_2/CC$ and $Al_2O_3/SnO_2/CC$ cells before and after 100 cycles is characterized and shown in Figure 5a and b. For the fresh $C/SnO_2/CC$ cell, the contact resistance is as small as 5 Ω and the charge transfer resistance of was calculated to be 165 Ω based on the semicircle [32]. After 100 cycles, the contact and charge transfer resistance increased to 20 Ω and 191 Ω. Meanwhile, the fresh $Al_2O_3/SnO_2/CC$ cell have a 372 Ω charge transfer resistance and a 105 Ω contact resistance, the increased contact and charge transfer

resistance can be attributed to the dense and insulating nature of the Al_2O_3 coating. After 100 cycles, the charge transfer resistance calculated from the first semicircle almost remains the same, however, the contact resistance increased to 175 Ω, and another big semicircle with a 450 Ω charge transfer resistance appears following the first semicircle, which implies a strong solid electrolyte interface (SEI) film already formed on the Al_2O_3 surface. In order to prove that hypothesis and gain insight into the capacity fading mechanism, SEM images of two samples with different surface coatings are obtained after washed with PC and DI water carefully to remove the Na salt. In Figure 5c, there is no obvious SEI film on the surface of the $C/SnO_2/CC$ sample after cycling. However, as we expected, SnO_2 nanocrystals agglomerated together and became porous bulks. Parts of the active material layer also detached from the carbon cloth, which should be considered as the main reason to the capacity decay of $C/SnO_2/CC$ sample. In the SEM image of the $Al_2O_3/SnO_2/CC$ sample after cycling, no obvious agglomerates and detachments were found, and a significant SEI film was observed at the same time, which gradually started to decompose after exposing to the electron beam for tens of seconds. Since the washing process for both samples are the same, we believe that the SEI film formed on Al_2O_3 surface has different composition or a larger thickness than that on the carbon coating surface. The different SEI film observed from Al_2O_3 coated sample may be formed because of the unique surface property of Al_2O_3 layer or the physical and electrochemical reaction between the electrolyte and Al_2O_3 surface coating. It is obvious that although the Al_2O_3 coating together with strong SEI film leads to the increasing of the contact and charge transfer resistance of $Al_2O_3/SnO_2/CC$ electrode, on the other hand, they provide the superior mechanical support to the SnO_2 active layer and suppress the volume change and pulverization of SnO_2 layer during sodiation and de-sodiation process. Compared to $C/SnO_2/CC$ sample, the strong SEI film on Al_2O_3 surface also consumes more Na-ion during sodiation process and results in a lower Coulombic efficiency during cycling as shown in Figure 4a.

Conclusions

In summary, hierarchical core–shell nanocomposite anode consisting of individual conductive carbon fiber, a SnO_2 intermediate layer and carbon or Al_2O_3 surface coating, was fabricated by hydrothermal and ALD method. The $Al_2O_3/SnO_2/CC$ anode maintained a 371 mA h/g specific charge capacity at 100th cycle which demonstrated superior electrochemical stability and the $C/SnO_2/CC$ anode delivered a 342 mA h/g and a 144 mA h/g capacity at 10 C and 30 C high charge/discharge current rate. The conductive soft platform as well as the precise hierarchical control of various sublayers of materials in designed order was believed to function synergistically to maintain an anode host mechanically, electronically, and electrochemically active and stable, despite its large volume change upon sodiation/desodiation cycles and semiconductor material nature. In particular, the designed surface-coating/nanocrystal-active-material-layer/soft-platform core–shell electrode system minimized the stress of the volume change and maximized the Na-ion transport kinetics of SnO_2 anode, which have been two rather severe challenges that this kind of Na-ion host is facing. The excellent rate capability and cycling stability, the easy processability of carbon fibers and the mature hydrothermal synthesis and ALD technology make this surface-coating/nanocrystal-active-material-layer/soft-platform core shell system an excellent candidate for Na-ion storage. Although Na-ion batteries has a great potential for the low-cost and material-abundant large scale energy storage application, we believe the fast charge/discharge capability is very meaningful to keep a high power density to match with several high power cathodes for full Na-ion batteries [33–35] The superior cycling performance, the excellent rate capability combined with the simplicity of the fabrication process, represents a new strategy for the development of inexpensive and versatile synthesis techniques for Na-based energy storage applications.

Acknowledgments

We would like to acknowledge the collaboration of this research with King Abdul-Aziz City for Science and Technology (KACST) via The Center of Excellence for Nanotechnologies (CEGN). We acknowledge the funding support from the University of Southern California, United States. A portion of the images and data used in this article were acquired at The Center for Electron Microscopy and Microanalysis, University of Southern California. We would like to thank Mr. Guangtong Zeng and Prof. Stephen Cronin for the impedance measurement.

Appendix A. Supporting information

Supplementary data associated with this article can be found in the online version at http://dx.doi.org/10.1016/j.nanoen.2015.07.010.

References

[1] P.G. Bruce, B. Scrosati, J.-M. Tarascon, Angew. Chem. Int. Ed. 47 (2008) 2930–2946.
[2] M. Ge, X. Fang, J. Rong, C. Zhou, Nanotechnology 24 (24) (2013) 1–10.
[3] J.P. Parant, R. Olazcuaga, M. Devalette, C. Fouassier, J. Solid State Chem. 3 (1971) 1–11.
[4] N. Yabuuchi, M. Kajiyama, J. Iwatate, H. Nishikawa, S. Hitomi, R. Okuyama, R. Usui, Y. Yamada, S. Komaba, Nat. Mater. 11 (2012) 512–517.
[5] S.M. Oh, S.T. Myung, J. Hassoun, B. Scrosati, Y.K. Sun, Electrochem. Commun. 22 (2012) 149–152.
[6] B.L. Ellis, W.R.M. Makahnouk, Y. Makimura, K. Toghill, L. F. Nazar, Nat. Mater. 6 (2007) 749–753.
[7] Y. Lu, L. Wang, J.B. Goodenough, Chem. Commun. 48 (2012) 6544–6546.
[8] C.D. Wessells, S.V. Peddada, R.A. Huggins, Y. Cui, 11(2011), 5421-5425.
[9] S.P. Ong, V.L. Chevrier, G. Hautier, A. Jain, C. Moore, S. Kim, X. Ma, G. Ceder, Energy Environ. Sci. 4 (2011) 3680–3681.
[10] C. Deng, S. Zhang, Z. Dong, Y. Shang, Nano Energy 4 (2014) 49–55.

[11] J. Qian, Y. Chen, L. Wu, Y. Cao, X. Ai, H. Yang, Chem. Commun. 48 (2012) 7070–7072.
[12] H. Song, N. Li, H. Cui, C. Wang, Nano Energy 4 (2014) 81–87.
[13] V.L. Chevrier, G. Ceder, J. Electrochem. Soc. 158 (2011) A1011–A1014.
[14] Y. Liu, Y. Xu, Y. Zhu, J.N. Culver, C.A. Lundgren, K. Xu, C. Wang, ACS Nano 7 (2013) 3627–3634.
[15] H. Zhu, Z. Jia, Y. Chen, N. Weadock, J. Wan, O. Vaaland, X. Han, T. Li, L. Hu, Nano Lett. (2013) 3093–3100.
[16] M.D. Slater., D. Kim, E. Lee, C.S. Johnson, Adv. Funct. Mater. 8 (2012) 947–958.
[17] Y. Wang, D. Su, C. Wang, G. Wang, Electrochem. Commun. 29 (2013) 8–11.
[18] D. Su, H.-J. Ahn, G. Wang, Chem. Commun. 49 (2013) 3131–3133.
[19] K. Kadirvelu, C. Faur-Brasquet, P. Le Cloirec, Langmuir 16 (2000) 8404–8409.
[20] Y. Liu, W. Zhang, Y. Zhu, Y. Luo, Y. Xu, A. Brown, J.N. Culver, C. A. Lundgren, K. Xu, Y. Wang, C. Wang, Nano Lett. 13 (2013) 293–300.
[21] B. Liu, J. Zhang, X. Wang, G. Chen, D. Chen, C. Zhou, G. Shen, Nano Lett. 12 (2012) 3005–3011.
[22] M. Gu, A. Kushima, Y. Shao, J.-G. Zhang, J. Liu, N.D. Browning, J. Li, C. Wang, Nano Lett. 13 (2013) 5203–5211.
[23] M. Ge, Y. Lu, P. Ercius, J. Rong, X. Fang, M. Mecklenburg, C. Zhou, Nano Lett. 14 (2014) 261–268.
[24] L.F. Cui, R. Ruffo, C.K. Chan, H. Peng, Y. Cui, Nano Lett. 9 (2009) 491–495.
[25] X. Fang, M. Ge, J. Rong, Y. Che, N. Aroonyadet, X. Wang, Y. Liu, A. Zhang, C. Zhou, Energy Technol. 2 (2014) 159–165.
[26] L.A. Riley, S.A. Cavanagh, S.M. George, S.-H. Lee, A.C. Dillon, Electrochem. Solid-State Lett. 14 (2011) A29–A31.
[27] M. Winter, J.O. Besenhard, Electrochim. Acta 45 (1999) 31–50.
[28] Y. He, X. Yu, Y. Wang, H. Li, X. Huang, Adv. Mater. 23 (2011) 4938–4941.
[29] X. Xiao, P. Lu, D. Ahn, Adv. Mater. 23 (2011) 3911–3915.
[30] P.L. Taberna, S. Mitra, P. Poizot, P. Simon., J.M. Tarascom, Nat. Mater. 5 (2006) 567–573.
[31] N. Balke, S. Jesse, Y. Kim, L. Adamczyk, A. Tselev, I.N. Ivanov, N.J. Dudney, S.V. Kalinin, Nano Lett. 10 (2010) 3420–3425.
[32] M. Gaberscek, R. Dominko, S. Pejovnik, M. Gabersceka, J. Electrochem. Soc. 157 (2010) A1218–A1228.
[33] P. Barpanda, T. Ye, S.I. Nishimura, S.C. Chung, Y. Yamada, M. Okubo, H. Zhou, A. Yamada, Electrochem. Commun. 24 (2012) 116–119.
[34] J. Qian, M. Zhou, Y. Cao, X. Ai, H. Yang, Adv. Energy Mater. 2 (2012) 410–414.
[35] L. Wang, Y. Lu, J. Liu, M. Xu, J. Cheng, D. Zhang, J. B. Goodenough, Angew. Chem. Int. Ed. 52 (2013) 1964–1967.

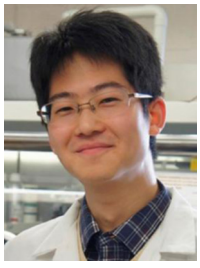

Yihang Liu is currently pursuing his Ph.D. under the supervision of Prof. Chongwu Zhou in Ming Hsieh Department of Electrical Engineering at University of Southern California. He received a master degree in Chemical Engineering from University of Maryland, College Park and a bachelor degree in Opto-Electronic Engineering from Beijing Institute of Technology, China. His research interests are energy storage devices, including Li-ion and Na-ion batteries.

Xin Fang received her Bachelor's degree from University of Science and Technology of China in 2010. She is currently pursuing her Ph.D. under the supervision of Prof. Chongwu Zhou in Mork Family Department of Chemical Engineering and Materials Science, University of Southern California. Her research mainly focuses on synthesis and modification of materials for energy storage and semiconductor devices.

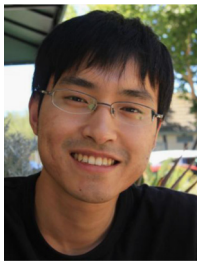

Mingyuan Ge is currently a Ph.D. student in the Mork Family Department of Chemical Engineering and Materials Science at University of Southern California. He received his bachelor's degree in Materials Science from Zhejiang University, China. His research interests focus on the synthesis and physical property study of nanostructured materials for energy-related application, such as Li-ion batteries and artificial photosynthesis.

Jiepeng Rong received his Bachelor's degree from University of Science and Technology Beijing in 2008, and Master's degree from University of Delaware in 2010. He is currently pursuing his Ph.D. under the supervision of Prof. Chongwu Zhou in Mark Family Department of Chemical Engineering and Materials Science, University of Southern California. His research mainly focuses on silicon-based anode materials and sulfur-based cathode materials for rechargeable lithium batteries.

Chenfei Shen received his Bachelor's degree from Department of Materials Science at Nanjing University of Aeronautics and Astronautics in 2011 and Master's degree from University of California, Los Angeles in 2012. He is currently pursuing his Ph.D. under the supervision of Prof. Chongwu Zhou at Mork Family Department of Chemical Engineering and Materials Science, University of Southern California. His research interests mainly focus on energy storage devices.

Anyi Zhang received his Bachelor's degree from the Department Chemical Engineering at Zhejiang University in 2011 and Master's degree from the Mork Family Department of Chemical Engineering and Materials Science at University of Southern California in 2013. He is currently pursuing his Ph.D. under the supervision of Prof. Chongwu Zhou at Mark Family Department of Chemical Engineering and Materials Science, University of Southern California. His research interests mainly focus on lithium-sulfur batteries.

Dr. Enaya is currently an Assistant Research Professor in The Center of Excellence for Green Nanotechnologies at KACST and UCLA. His current research focuses on high frequency nano devices, nano-enabled energy storage, and spintronics. Dr. Enaya is also a co-founder of Carbonics, a startup that provides RF semiconductor solutions to cope with the higher frequency and tough linear requirements for next generation wireless products. Dr. Enaya received his B.S. and Ph.D. in Electrical Engineering from North Carolina State University, where he joined Dr. Ki Wook Kim group to investigate nonvolatile spin memory devices based on diluted magnetic semiconductors.

Dr. Chongwu Zhou is a full professor of Department of Electrical Engineering at University of Southern California (USC). He previously held positions of Jack Munushian Associate Professor (2006–2011) and Assistant Professor (2000–2006) at USC. He received Bachelor's Degree from the University of Science and Technology of China in 1993, received Ph.D. in Electrical Engineering from Yale University in 1999, and worked as a postdoc at Stanford University from 1998 to 2000. His research interest covers nanomaterials, nanoelectronics, energy nanotechnology, and bionanotechnology. He is an Associate Editor for Nanotechnology and IEEE Transactions on Nanotechnology, and serves as an Editorial Advisory Board member for ACS Nano.